RSC Advances

PAPER

View Article Online
View Journal | View Issue

Cite this: *RSC Adv.*, 2017, **7**, 54522

Fabrication of a new metal–organic framework for sensitive sensing of nitroaromatics and efficient dye adsorption†

Wei-Ping Wu,*[a] Jian Wu,[b] Jian-Qiang Liu,*[c] Manoj Trivedi[d] and Abhinav Kumar*[e]

Received 11th October 2017
Accepted 23rd November 2017

DOI: 10.1039/c7ra11221a

rsc.li/rsc-advances

The hydrothermal reaction of Cd(II) salt with rigid tetracarboxylate ligand, terphenyl-3,3″,5,5″-tetracarboxylic acid (H_4L) produced a new metal–organic framework (MOF) $\{[Cd_2(L)(DMF)_3]\cdot 0.5DMF\}_n$ (**1**). Single crystal X-ray diffraction showed that MOF **1** possesses a 3D microporous framework with 4-connected **Dia** topology which is based on $\{Cd_2(CO_2)_4\}$ subunits. MOF **1** is a promising dual functional sensor with high selectivity and sensitivity for the detection and recognition of nitroaromatics (NACs) and Fe^{3+} ions *via* alleviation of its fluorescence intensity. Furthermore, **1** also has an excellent capacity to adsorb methylene blue (MB) with high selectivity, and it retains almost similar adsorption performance after being recycled several times. The observed decrease in fluorescence intensity of **1** in the presence of NACs has been addressed by theoretical calculations which indicate that the intensity alleviation of **1** in the presence of NACs can be attributed to an electron and resonance energy transfer between **1** and nitro analytes.

The continuous and exponential misuse of nitro-aromatic compounds (NACs) as explosives has led to countless economic losses to the world because of their explosive nature.[1] Thus, precise and effective detection of these explosive compounds is vital for civil security. The traditional detection methods for detecting these molecules by using state-of-the-art analytical instruments have emerged and they have displayed good performance.[2,3] However, these methods suffer from drawbacks *viz.* high equipment costs and poor portability which prevent their widespread applications.[4] Recently, luminescent metal–organic frameworks (LMOFs) have been widely employed in building optical sensors because they can encapsulate the analytes and exhibit luminescence quenching or spectrum shifting. Hence LMOFs have gained a reputation as being cheap, fast and portable systems for the effective detection of analytes *viz.* ions and molecules.[5] Also, it has been established that the luminescence properties of LMOFs can be tuned by using different ligands having rigid organic moieties and the resultant LMOFs can in turn be utilized for the specific detection of ions and molecules.[6–10]

The waste-water discharge always comprises of significant amount of organic dyes which imposes significant threat to the environment and human health because of the toxic and carcinogenic properties associated with these organic dyes.[11] Until now, many approaches for the removal of dyes for example using activated carbons and zeolites *etc.* have been applied during the industrial processing of the waste-water.[11] But they display poor performance when selective removal of the targeted organic dye from waste-water containing mixture of organic molecules is concerned.[12] Therefore, the design and synthesis of porous MOFs having selective adsorption of molecule for waste-water treatment applications is highly desirable.[12]

With these viewpoints and in our continuous quest for the development of new LMOFs[13] for sensing applications for the detection nitro-aromatics as well as dye-adsorption, in the presented work, we had used a rigid multicarboxylate terphenyl-3,3″,5,5″-tetracarboxylic acid (H_4L) to fabricate d^{10}-based Cd(II) LMOFs. The use of this ligand is based on the following associated features:[14] (a) H_4L comprises of four carboxylic acid groups and therefore have multiple coordination sites and hence can display varied coordination modes and in-turn is capable of yielding high dimensional frameworks; (b) the use of symmetry linkers sometimes has been shown to be an effective

[a]*College of Chemistry and Environmental Engineering, Sichuan University of Science & Engineering, Zigong 643000, P. R. China. E-mail: wuweipingzg@126.com*

[b]*Guangxi Key Laboratory of Chemistry and Engineering of Forest Products, Guangxi University for Nationalities, College of Chemistry and Chemical Engineering, Nanning, Guangxi 530006, China*

[c]*Dongguan Key Laboratory of Drug Design and Formulation Technology, Key Laboratory of Research and Development of New Medical Materials of Guangdong Medical University, School of Pharmacy, Guangdong Medical University, Dongguan, 523808, P. R. China. E-mail: jianqiangliu2010@126.com*

[d]*Department of Chemistry, University of Delhi, Delhi, India*

[e]*Department of Chemistry, Faculty of Science, University of Lucknow, Lucknow 226 007, India. E-mail: abhinavmarshal@gmail.com; kumar_abhinav@lkouniv.ac.in; Fax: +91-769-22896560; Tel: +91-769-22896560*

† Electronic supplementary information (ESI) available. CCDC 1556532. For ESI and crystallographic data in CIF or other electronic format see DOI: 10.1039/c7ra11221a

way to suppress framework interpenetration and promote the formation of porous materials.[3c] In this work Cd(II) MOF **1** possess a 3D framework having 4-connected **Dia** topology and can be used as a luminescent sensor for the detection of nitro-aromatics (NACs) and Fe^{3+} as well as an effective adsorbent for methylene blue (MB).

Materials and method

General considerations

All the chemicals were available commercially and have been used without any further purification. Powder X-ray diffraction (PXRD) data for **1** was collected using Bruker D8 Advance X-ray diffractometer equipped with Cu-Kα radiation ($\lambda = 1.5418$ Å) at 50 kV, 20 mA with a scanning rate of 6° min^{-1} and a step size of 0.02°. The simulated powder patterns of **1** were obtained using Mercury 2.0 which was compared with the experimental PXRD to check the purity and homogeneity of **1** in bulk. FT-IR spectra as KBr pellet were measured using a Nicolet Impact 750 FTIR in the range of 4000–400 cm^{-1}. Thermogravimetric analysis was performed under nitrogen atmosphere from room temperature to 650 °C at a heating rate of 10 °C min^{-1}, using a SDT Q600 thermogravimetric analyzer.

X-ray crystallography

The single crystal X-ray diffraction data collection for **1** was carried out using Bruker SMART APEX diffractometer that was equipped with a graphite monochromated Mo-Kα radiation ($\lambda =$ 0.71073 Å) by using an ω-scan technique. The intensities of the absorption effects were corrected by using SADABS. The structure was solved by direct method (SHLEXS-2014) and refined by full-matrix least-squares procedure based on F^2 (SHELXL-2014).[15] All the hydrogen atoms were generated geometrically and refined isotropically using the riding model. The MOF **1** was weakly diffracting in nature and hence gave poor data. Thus, restraints were applied during the refinement of the structure using the restraint commands (SIMU, SADI and EADP *etc.*), which have been used for some unreasonable atoms. Because guest molecules (DMF) in the channels of **1** were highly disordered and those could not be modelled properly, the SQUEEZE routine of PLATON was applied to remove their contributions.[16] All non-hydrogen atoms were refined with anisotropic displacement parameters. Crystallographic details and selected bond dimensions for **1** are listed in Tables S1 and S2,† respectively. CCDC number: 1556532.

Synthesis of $[Cd_2(L)(DMF)_3]\cdot 0.5DMF\}_n$ (1)

A mixture of terphenyl-3,3″,5,5″-tetracarboxylic acid (H_4L) (0.1 mmol, 0.018 g) and $Cd(NO_3)_2\cdot 6H_2O$ (0.2 mmol, 0.042 g) was dissolved in DMF (2 mL) in a screw-capped vial and two drops of HNO_3 (65%, aq) was added to the mixture. The obtained solution was placed in a 25 mL vial and heated to 85 °C for 72 h. After that the reaction mixture was cooled to room temperature at a rate of 2 °C h^{-1}. Colorless block crystals of **1** were obtained in 39% yield based on Cd. Anal. (%) calcd for $C_{32.5}H_{34.5}O_{11.5}N_{3.5}Cd_2$: C, 44.21%; H, 3.94%; N, 5.55%; found: C, 43.88%; H, 3.83%; N, 5.46%. IR: 2340 (m); 1646 (vs); 1598 (m); 1540 (vs); 1345 (vs); 1288 (m); 1106 (m); 916 (m); 778 (v); 725 (v); 661 (m).

Computational details

The mechanism associated with the alleviation in the fluorescence intensity of **1** in the presence of NACs have been proposed using density functional theory (DFT) calculations. The optimized molecular geometries different analytes, the ligand H_4L as well as MOF **1** were calculated using the B3LYP exchange–correlation functional.[17a,b] The 6-31G** basis set for all the atoms other than Cd was used and for Cd LANL2DZ basis set was employed. All the calculations were performed using Gaussian 09 programme.[17c]

Results and discussion

$[Cd_2(L)(DMF)_3]\cdot 0.5DMF\}_n$ (1)

The asymmetric unit in MOF **1** comprises of one L^{4-} ligand, two Cd(II) ions, three coordinated DMF molecules, and a free half DMF molecule (Fig. 1a). There are two crystallographically independent Cd(II) centers (Cd1 and Cd2) existing in different coordination environments. Cd1 is coordinated to four oxygen atoms of the two chelating carboxylate groups (O1, O2, O3 and O4) and two oxygen atoms from two bridging-bidentate carboxylate groups (O5 and O7) thereby completing a distorted octahedral environment (Fig. 1a). The Cd2 center also possess distorted octahedral coordination geometry in which the axial sites are occupied by one oxygen atom from one bridging-bidentate carboxylate group (O6) and one oxygen atom from coordinated DMF (O10). The equatorial positions are occupied by O1 and O8 atoms from two L^{4-} linkers and O9 and O11 of DMF molecules. The two L^{4-} linkers lie across twofold axes and display two coordination modes (Scheme S1†). The two unique Cd(II) centers are bridged by three carboxylate groups which leads to the formation of a dinuclear cluster (Fig. 1b). The L^{4-} ligands bridges the $Cd_2(CO_2)_4$ clusters to generate a 3D network (Fig. 1c and S1†). Each cluster is coordinated to four L ligands, and each L ligand binds to four clusters. Thus the cluster and both unique L^{4-} ligands act as 4-c nodes, and generate an underlying network with the diamond topology (Fig. 1d).[18,19] There is the formation of a 3D framework that exhibits elliptical channels of dimension 8.1 × 10.2 $Å^2$ along the *c* crystallographic direction (atom-to-atom separations). The disordered DMF solvent molecules are located in these channels. The differences in the topologies of the MOFs synthesized using H_4L ligand can be attributed to the variation in the feature of cluster modes.[20] The calculations using PLATON indicates that the effective free volume in **1** is ~68.7%.[16]

The thermogravimetric analysis indicates that the framework of **1** is stable up to 350 °C (Fig. S2†). The permanent porosity of the framework of **1** had been estimated using N_2 adsorption profile (Fig. S3†) which indicates that **1** is a microporous material with pore volume of 115.50 cm^3 (STP) g^{-1} and the BET surface area is 320.5 m^2 g^{-1}.[21]

Fluorescence sensing

The fluorescence properties of both **1** and H_4L ligand were investigated in the solid state. On excitation at ~280 nm, both **1**

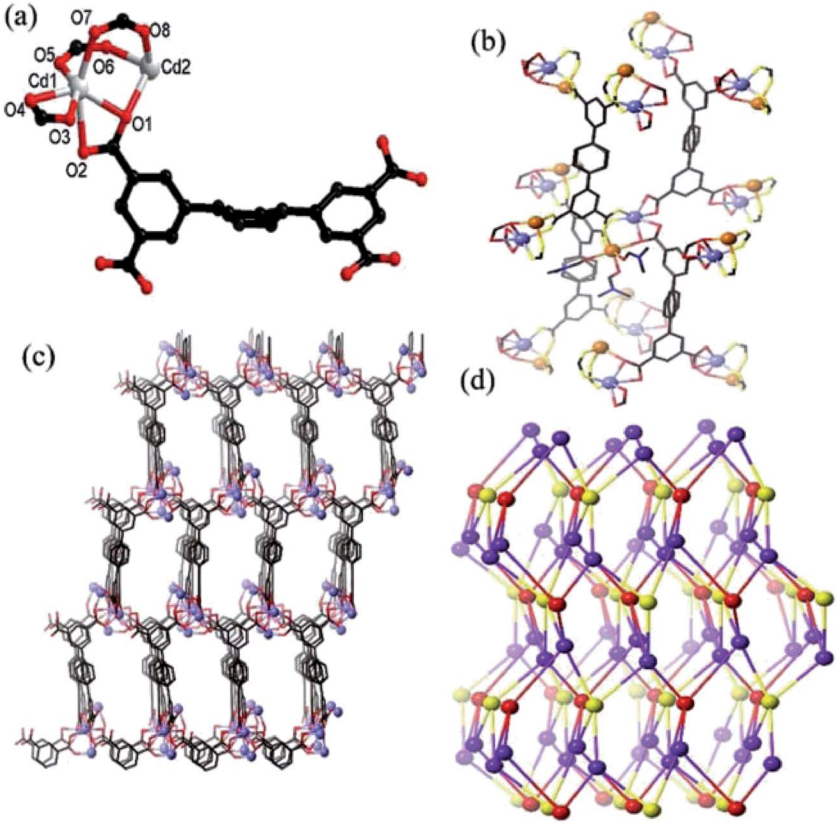

Fig. 1 (a) The perspective view of the coordination geometries of Cd(II) centres in **1**; (b) local coordination environments of both the ligand and the Cd_2 metal cluster in **1**. For clarity, the two unique Cd(II) centers are shown in different colours (Cd1 in purple, Cd2 in orange), the oxygen atoms of the two unique L ligands are shown in different colours (red or yellow). (Hydrogen atoms have been omitted for clarity. The central aromatic rings of both L ligands are disordered over two positions.) (c) The perspective view of the 3D network in **1**; (d) the underlying distorted diamond (**dia**) net in the structure of **1**; red and yellow spheres represent the two different ligand nodes, while purple spheres represent the Cd_2 cluster nodes (although all nodes are topologically equivalent).

and H_4L displayed strong emissions at ~375 nm and 455 nm, respectively but the intensity in emission of **1** was quite strong while that of H_4L was weak (Fig. S4†). The observed emission band in **1** could be tentatively attributed to the intra-ligand charge transfer (ILCT), which are constrained by coordination to Cd^{2+} with a relatively short distance between adjacent H_4L ligands, improving the weak interactions between them and thus change the emission.[22] The intense emissive response of **1** in solid state stimulated us to explore its potential as possible fluorescent sensor for nitro-aromatic. The fluorescence property of **1** as suspensions in different solvents were examined and the suspension of **1** in nitrobenzene displayed the emission with lowest intensity. The observed emissive property of **1** as suspension in nitrobenzene was entirely different from the suspension of **1** in other solvents (Fig. 2a and S5†). Hence the suspension of **1** in DMF was used for the detection of different aromatics and nitro-aromatics *viz.* 2,4,6-trinitrophenol (TNP), 2,4-dinitrotoluene (2,4-DNT), 2,6-dinitrotoluene (2,6-DNT), 2-nitrotoluene (2-NT), 4-nitrotoluene (4-NT), 1,3-dinitrobenzene (1,3-DNB), 1,2,4-trimethylbenzene (1,2,4-TMB), 1,3,5-trimethylbenzene (1,3,5-TMB), *o*-nitrophenol (MNP), *p*-nitrophenol (PNP), 2,4-dinitrophenol (2,4-DNP). All the twelve aromatics compounds were capable of alleviating the emission intensity of **1** but to a different extent. The order of quenching efficiency of aromatics is 2,4-DNP > PNP ≈ MNP > TNP > 4-NT > 2-NT > 2,4-DNT > 2,6-DNT > NB > 1,3-DNB > 1,2,4-TMB > 1,3,5-TMB (Fig. 2b).[23] Furthermore, the fluorescence intensity decreases steadily with concomitant increase in the concentrations of 2,4-DNP, PNP, MNP and TNP. Upon addition of 90, 600, 240 and 500 ppm of 2,4-DNP, PNP, MNP and TNP, respectively, the luminescent intensity of **1** was observed to be nearly nullified (Fig. 2c–e and S6–S9†).[24]

The other nitro-aromatics also displayed quenching effect to different extent on the fluorescence intensity of **1** (Fig. S10–S21†). These results demonstrated that **1** possess good selectivity to detect 2,4-DNP, PNP, MNP and TNP in presence of other NACs (Fig. 2c–f and S6–S9†). The quantitative fluorescence quenching efficiency can be explained with the help of Stern–Volmer (SV) equation: $(I_0/I) = 1 + K_{sv}[Q]$ and it is observed that the Stern–Volmer plots for 2,4-DNP, PNP, MNP and TNP are nearly linear when the concentrations of these NACs are at low concentrations with the corresponding K_{sv} values of 3.01×10^4, 7.47×10^3, 6.55×10^3 and 1.08×10^4 M^{-1}, respectively (Fig. S6–S9†). The 2,4-DNP, PNP, MNP and TNP detection limits are calculated to be 0.89, 1.75, 1.66 and 1.64 ppm, respectively. Therefore, from this observation it can be inferred that **1** can be

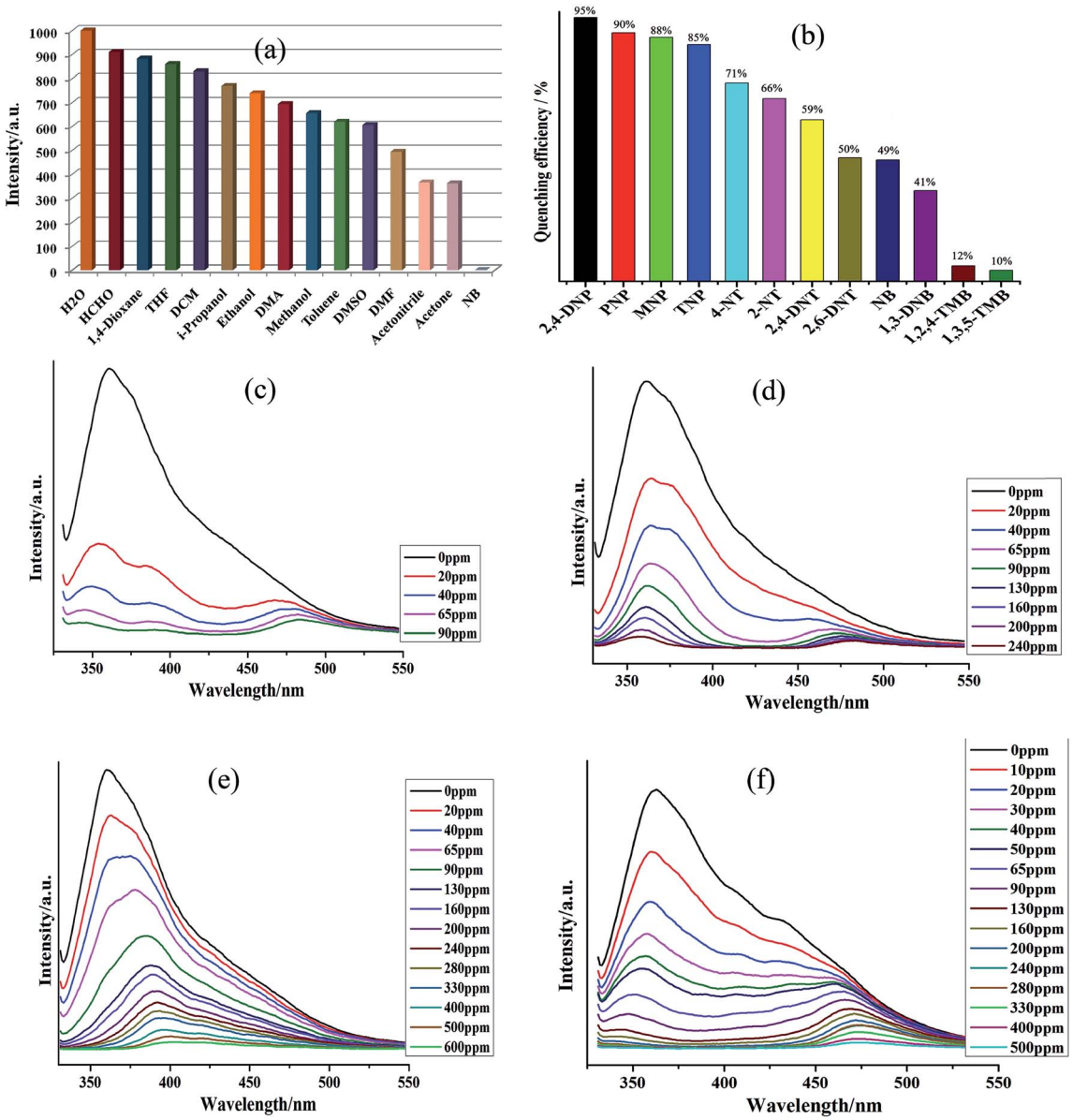

Fig. 2 (a) Photoluminescence intensity of **1** dispersed in different solvents, excited at 280 nm; (b) the quenching efficiency of **1** dispersed in different explosives; (c–f) photoluminescence intensity of **1** dispersed in 2,4-DNP, PNP, MNP and TNP, respectively, excited at 280 nm.

used to distinguish NACs having varied number of –OH groups in a mixture comprising of other aromatics. Further to elucidate the detection mechanism of the sensors, the luminescence sensing of H_4L emulsions in the presence of 2,4-DNP were measured (Fig. S22†). The emission intensity of H_4L remained almost unchanged with different concentrations of 2,4-DNP suggesting that there may be interactions operating between 2,4-DNP and the Cd(II) centers of **1** and the variation in emission intensity are not related to the between 2,4-DNP and the ligands H_4L.[25–27] Also, the results of the powder X-ray diffraction (PXRD) patterns (Fig. S27d†) indicated possible structural and/or symmetry changes within the crystal structure of **1** during the guest uptake.

The alleviation in the fluorescence intensity of **1** in the presence of ACs/NACs have been tried to be addressed with the aid of density functional theory calculations in which the HOMO–LUMO energies of all the ACs/NACs, **1** as well as H_4L have been computed at the B3LYP level (Table 1, Fig. S28†). Our previous investigations[13] indicated that the probable reason lying behind the fluorescence quenching of **1** in presence of NACs will be the charge transfer from **1** to the LUMO of the NACs. Additionally, this charge transfer will be viable only when the LUMO of donor MOF **1** is positioned at energetically higher position in comparison to LUMO of the acceptor ACs/NACs.[26–28] The computed HOMO–LUMO energies presented in Table 1 indicates that LUMO of all the NACs are lying at relatively lower energy when compared to donor **1** and as a consequence charge transfer from **1** to NACs can occur which may result in the decrease in fluorescence intensity in **1**. But the observed order of fluorescence alleviation in **1** by these NACs is not fully consistent with LUMO

Table 1 The HOMO–LUMO energies (in eV) for ligand (H_4L), MOF **1** and NACs

Ligand/analyte	HOMO	LUMO
H_4L	−6.36	−1.83
1	−5.73	−2.09
2-Nitrotoluene (2-NT)	−7.28	−2.32
4-Nitrotoluene (4-NT)	−7.36	−2.32
Nitrobenzene (NB)	−7.60	−2.43
2,6-Dinitrotoluene (2,6-DNT)	−7.91	−2.87
2,4-Dinitrotoluene (2,4-DNT)	−8.11	−2.98
1,3-Dinitrobenzene (1,3-DNB)	−8.42	−3.14
2,4,6-Trinitrophenol (TNP)	−8.54	−3.55
1,2,4-Trimethylbenzene (1,2,4-TMB)	−6.03	0.28
1,3,5-Trimethylbenzene (1,3,5-TMB)	−6.18	0.26
2,4-Dinitrophenol (2,4-DNP)	−7.62	−3.33
o-Nitrophenol (MNP)	−6.80	−2.72
p-Nitrophenol (PNP)	−7.43	−2.39

energy trends of NACs, which indicates that the charge transfer is not the sole phenomenon for the alleviation in the fluorescence intensity and there may be the existence of electrostatic interaction between the **1** and NACs which is also contributing to the fluorescence quenching.[13]

The metal ion interaction studies were also performed by addition of 1.0×10^{-4} M nitrate salts of Zn^{2+}, Cd^{2+}, Ca^{2+}, Al^{3+}, K^{+}, Na^{+}, Mg^{2+}, Ni^{2+}, Hg^{2+}, Pb^{2+}, Co^{2+}, Cu^{2+}, Ag^{+} and Fe^{3+} to **1**–H_2O emulsions. The fluorescence intensities of M^{n+}@**1** emulsions were recorded and compared (Fig. 3a and S23†) which indicated markedly different fluorescence intensities. Zn^{2+}, Cd^{2+} and Al^{3+} metal ions exhibited positive effects on the luminescent intensity, while others demonstrated different levels of quenching effect on luminescent intensity, especially Fe^{3+} exhibiting the most significant quenching effect.[28] The sensitivity of **1** towards Fe^{3+} was also explored further by performing the concentration gradient experiments by using the Fe^{3+} solutions having the concentration ranging from 0 to 600 ppm. The concentration gradient experiments indicated that the luminescence intensity of Fe^{3+}@**1** gradually decreases with the increase in concentration of Fe^{3+} (Fig. 3a). Furthermore, the fluorescence lifetime measurements indicated that the fluorescence lifetime of **1** which was in isolated state was 110.41 ns gets reduced to 8.19 ns in presence of 1.0 mM Fe^{3+} (Fig. S24†). Hence, it can be inferred that energy transfer may be responsible for the quenching phenomenon.[29] To elucidate the possible mechanism for such fluorescence quenching by Fe^{3+} ion, O 1s X-ray photoelectron spectroscopic (XPS) studies were

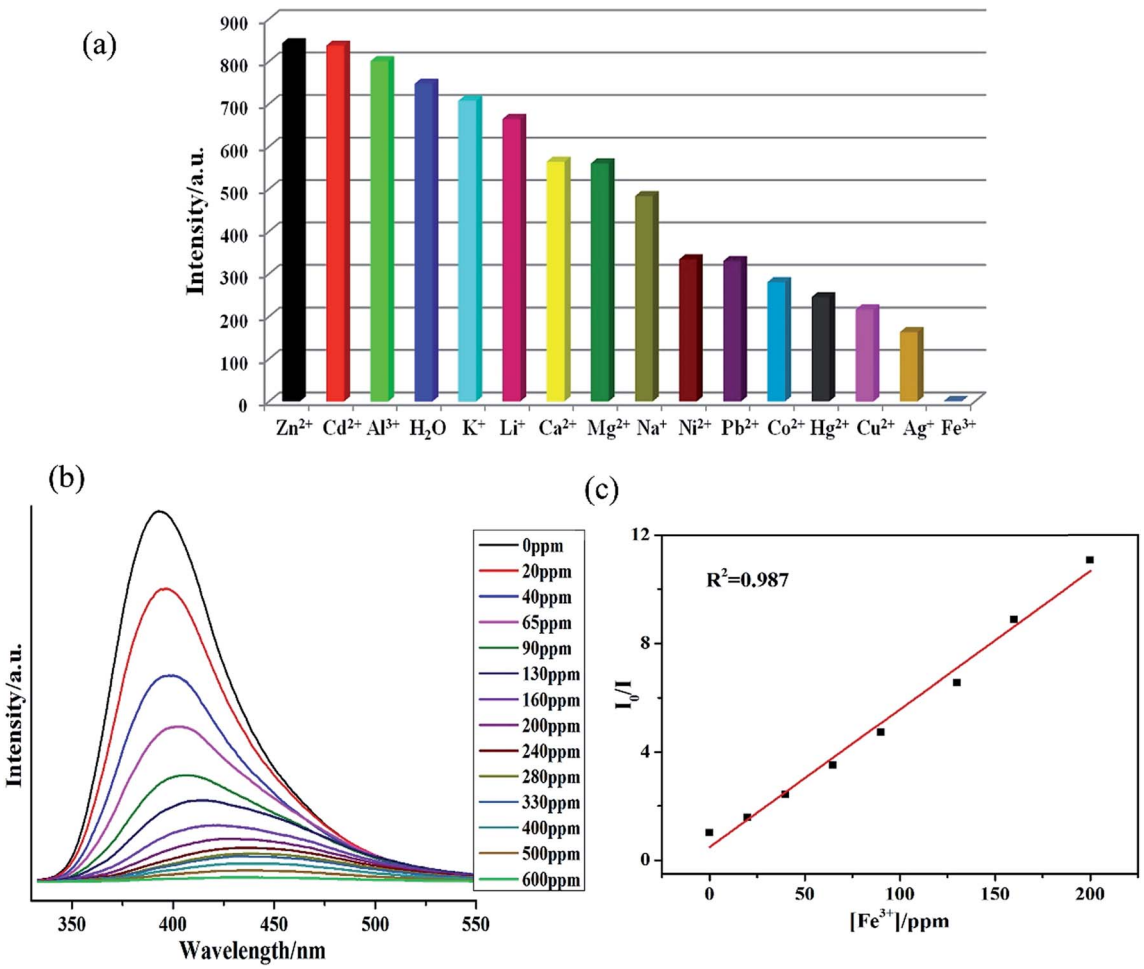

Fig. 3 (a) Photoluminescence intensity of **1** dispersed in different metal ions solutions, excited at 280 nm; (b) emissive response spectra of **1** for Fe^{3+} in H_2O solution with different concentrations; (c) the Stern–Volmer plot for Fe^{3+}.

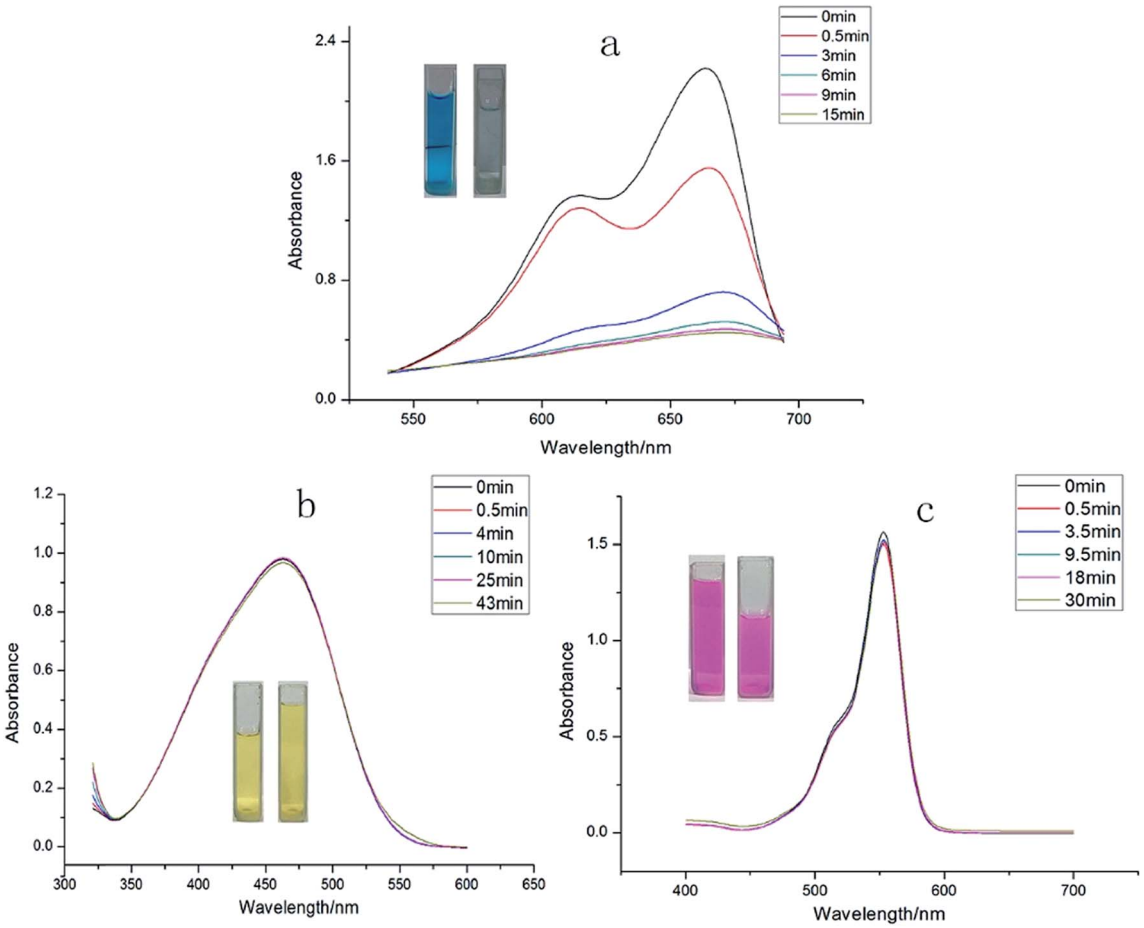

Fig. 4 The periodic UV-vis spectroscopy showing the adsorption capability of **1** toward (a) MB dye, (b) MO dyes, and (c) Rh B dye.

carried out on **1** and Fe^{3+}@**1**. XPS investigation indicated that the O 1s peak observed at 531.62 eV for the free oxygen atoms of the carboxylate ligand in **1** gets shifted to 531.74 eV on the addition of Fe^{3+} (Fig. S25a†), which may indicate the weak binding of oxygen atoms to Fe^{3+}. The powder X-ray diffraction (PXRD) patterns (Fig. S27c†) indicated possible structural and/or symmetry changes within the crystal structure of **1** upon dispersion in Fe^{3+} solutions.

The Stern–Volmer plots for Fe^{3+} are nearly linear at low concentrations ($R^2 = 0.987$) with the K_{sv} value of 2.06×10^4 M^{-1} (Fig. 3b). The Fe^{3+} detection limit is calculated to be 1.24 ppm. Fe^{3+} ion with the larger K_{sv} value demonstrates its quenching effect on the luminescent intensity of **1**.[29,30] As presented in Table S3,† most of the reported MOFs can detect Fe^{3+} in the concentration ranging between 10^{-3} to 10^{-5} M, and the lowest detected concentration of Fe^{3+} was recorded *ca.* 0.9×10^{-6} M.[29b] In comparison to these reports, **1** also display potentially high sensitivity and selectivity for Fe^{3+}.

Selective adsorption of organic dye

We also attempted to probe **1** as an adsorbent for different organic dyes present in the waste-water. As a model system three types of dye (methylene blue (MB), methyl orange (MO) and rhodamine B (Rh B)) with different size and charges were chosen as adsorbates.[31] In a typical experiment, 30 mg of adsorbent **1** was immersed in 30 mL of aqueous dye solution containing 1×10^{-5} mol L^{-1} of dye at room temperature and the mixture was continuously stirred. During the given time period, the ability of **1** to adsorb dyes from aqueous solution was determined through UV-vis spectroscopy. The UV-vis spectroscopy results showed that **1** possesses excellent capacity to adsorb MB (Fig. 4) while its ability to adsorb MO and Rh B was almost negligible. A plausible mechanism of the selective adsorption of MB by **1** could be explained through size matching of the MB molecule with the pore size of **1**.[32] The adsorption rate is greater than 75% in the first 30 s, moreover, it is worthy to mention that **1** can adsorb completely MB within 15 minutes.

The removed quantity of MB by **1** has been calculated using the following equation.[33–36]

$$Q_{eq} = \frac{C_0 - C_{eq}}{m} V \quad (1)$$

The equation indicates that every gram of **1** can adsorb 68.5 mg of MB. This fast and high-capacity adsorption process is also very important for adsorbents in practical wastewater treatment.[33] The color of the crystals of **1** was found to change from colorless to blue after adsorption (Fig. 5), which indicated

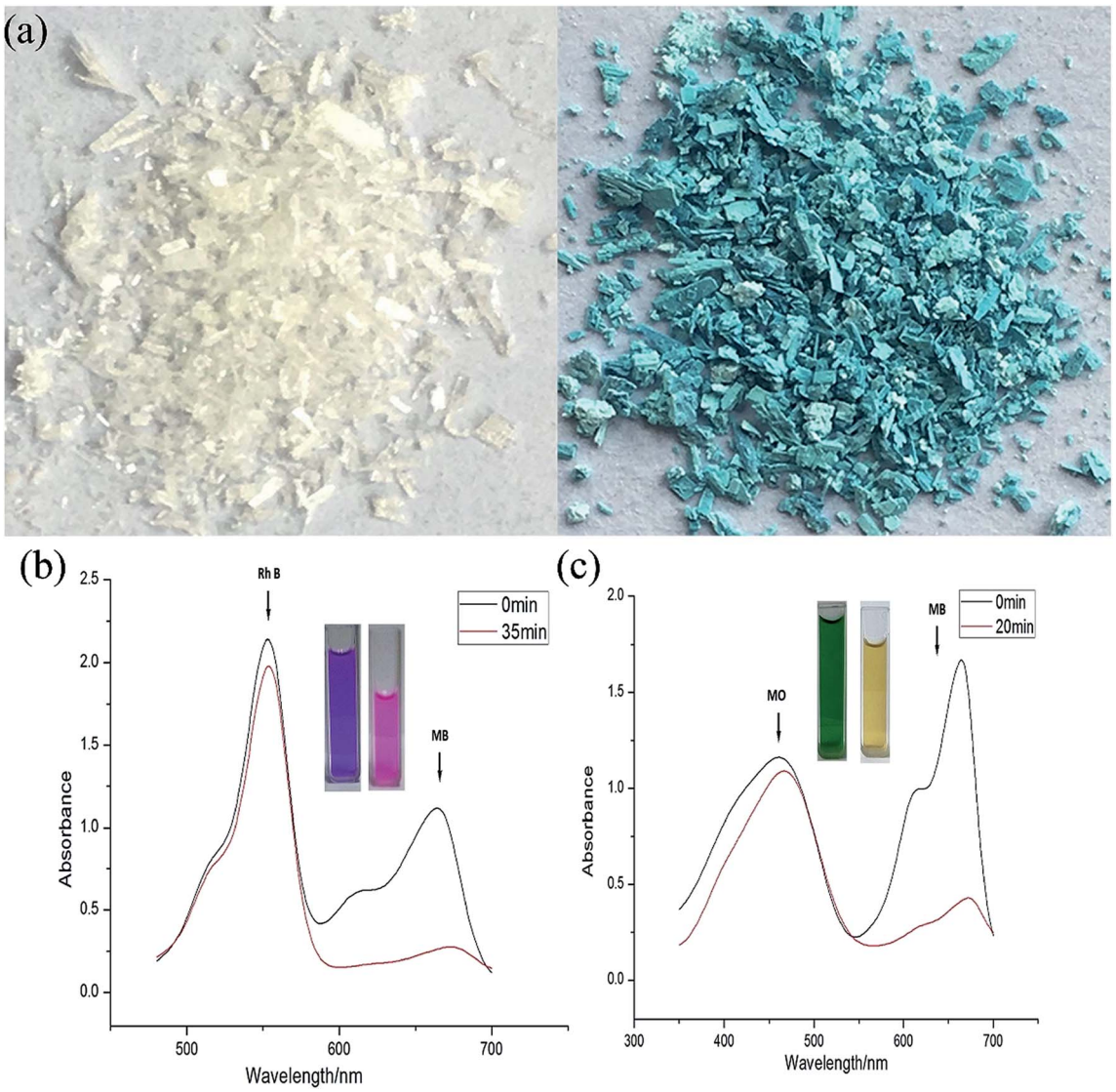

Fig. 5 (a) The color of **1** before (left) and after (right) adsorption of MB dye; (b) the adsorption capability of **1** toward Rh B + MB mixed dyes; (c) MB + MO mixed dyes.

Table 2 Kinetics parameters for different kinetics model for MB adsorption using **1**

Model	Parameter	MB
Pseudo-first-order	K_1 (min^{-1})	0.670
	q_e ($mg\ g^{-1}$)	47.55104
	R	0.97673
Pseudo-second-order	K_2 ($g\ mg^{-1}\ min^{-1}$)	0.01379
	q_e ($mg\ g^{-1}$)	39.573
	R	0.99446
Second-order	K_3 ($g\ mg^{-1}\ min^{-1}$)	2.17786
	q_e ($mg\ g^{-1}$)	0.1483
	R	0.49404
Intraparticle diffusion	K_4 ($mg\ g^{-1}\ min^{-1/2}$)	10.9904
	C	2.44444
	R	0.92411

that MB molecules entered into the crystal lattice of **1** instead of merely being getting adsorbed on the surface of the crystals.

To validate whether **1** possesses the ability to separate MB from a mixed-dye solution, we utilized **1** to capture MB from mixed-dye aqueous solutions. The UV-vis spectra were recorded after soaking **1** in mixed dye aqueous solutions comprising of Rh B + MB as well as MB + MO and it was observed that in both the cases only MB molecules could efficiently be adsorbed by **1** over a period of time (Fig. 5a and b), while Rh B and MO could not be encapsulated by **1**. As shown in the photographs (the inserted pictures in Fig. 5b and c), after soaking **1** in the mixed-dye aqueous solution, the color of the solution changed but finally retained the characteristic color of Rh B and MO. These results also confirms that **1** could effectively and selectively adsorb MB molecules into its framework and leaving Rh B as well as MO molecules in solution. Furthermore, the adsorption capacity of the **1** is fully maintained after recycling the MOF for

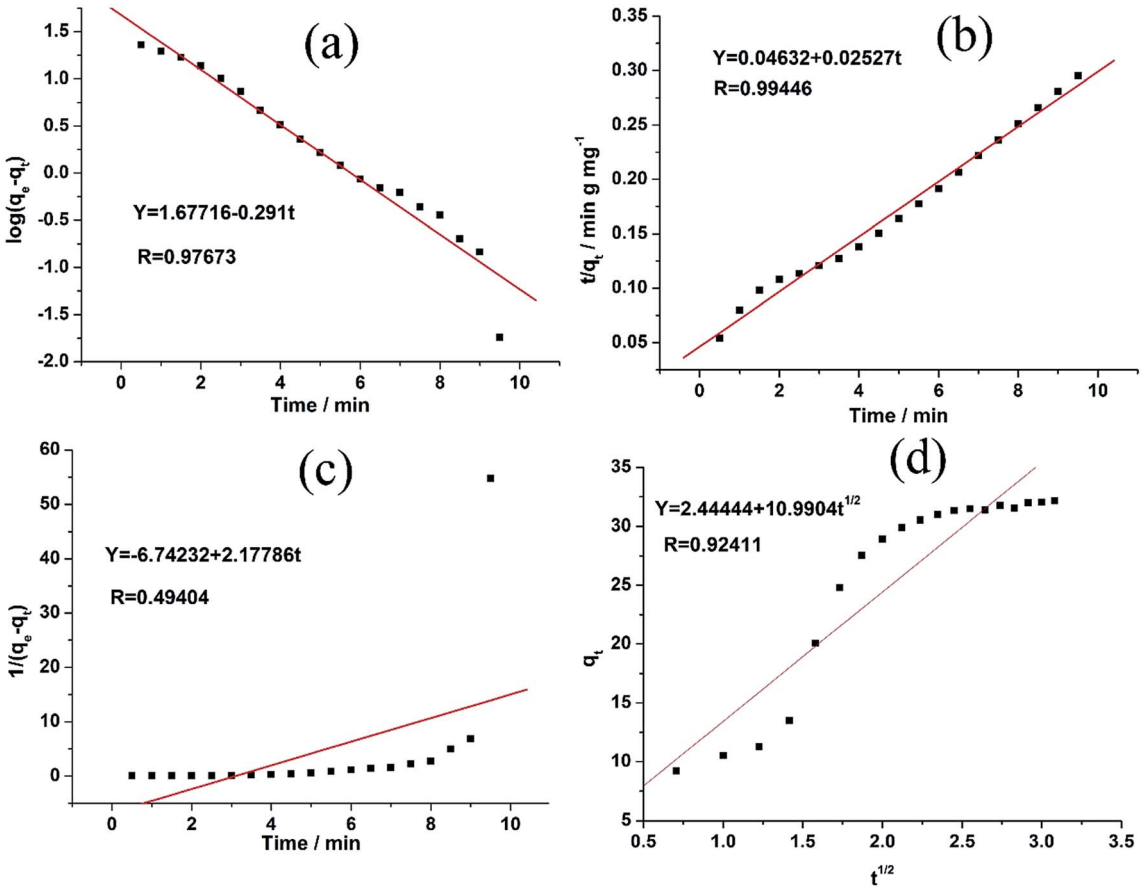

Fig. 6 (a–d) The adsorption kinetics of MB onto **1** using pseudo-second-order using different models, respectively.

five times. After adsorption, the MB@**1** can expediently release MB through simply washing the sample MB@**1** with ethanol after recycling 5 times and after releasing MB **1** again displayed almost identical rapid and quantitative adsorption of MB (Fig. S29†). Thus, **1** acts as an excellent candidate as a selective adsorption material, which can be applied practically to adsorb MB in waste-water containing mixture of organic dyes.

Adsorption kinetics

The rate of dye adsorption by **1** depends on the contact time of **1** and dye solution as well as on the diffusion process. During the process of adsorption, MB molecules migrate to the outer surface of **1**, diffuse into the layers of the MOF, and are then adsorbed *via* pore diffusion. To further explore the adsorption kinetics, pseudo-first order, pseudo-second-order, second-order and intra-particle diffusion kinetics models were employed. The constants of all of the kinetics models were calculated by using equations.

The pseudo-first-order rate equation:

$$\log(q_e - q_t) = \log q_e - \frac{K_1}{2.303}t \quad (2)$$

The pseudo-second-order rate equation:

$$\frac{t}{q_t} = \frac{1}{K_2 q_e^2} + \frac{t}{q_e} \quad (3)$$

The second-order rate equation:

$$\frac{1}{q_e - q_t} = \frac{1}{q_e} + K_3 t \quad (4)$$

$$q_t = K_4 t^{1/2} + C \quad (5)$$

As evident from the Table 2 and Fig. 6, there are four R^2 for MB obtained from the aforementioned equations. The fit of the experimental results show that the pseudo-second-order model possesses the highest R^2 value compared to the other adsorption kinetics models.[32,36] Therefore, the results indicate that the adsorption kinetics can be best described by a pseudo-second order model.

Conclusion

Our results indicated that the fluorescent MOF **1** reported herein possesses dual sensing ability for nitro-aromatics and ferric. The presented investigation indicated that the tetracarboxylate ligand terphenyl-3,3″,5,5″-tetracarboxylic acid (H_4L) because of its symmetric structure provides a new avenue to produce a new 3D microporous framework with 4-connected **Dia** topology based on $\{Cd_2(CO_2)_4\}$ subunits. The theoretical calculations indicated that not only charge transfer rather electrostatic interaction between the **1** and nitro-aromatic

compounds also contribute towards the exceptional selective fluorescence intensity alleviation. Also, **1** acted as an excellent and selective adsorbent material for organic dye methylene blue (MB) and can be utilized repeatedly for effective adsorption of MB from waste-water without significant alleviation in the adsorption capacity. It is apparent from the investigation that by choosing suitable symmetric polycarboxylate ligands one can develop LMOFs for selective sensing as well dye adsorption applications.

Conflicts of interest

There are no conflicts to declare.

Acknowledgements

This work was partially supported by the grants from the Science and Technology Plan Projects of Dongguan (2016108101005), Sichuan University of Science and Engineering (No. 2015RC26), Innovative Entrepreneurial Training Plan of undergraduates in Guangdong Province (20170571005, 20170571007, 201705710011, 20170571016, 20170571019, 20170571012, 20170571060, 20170571078), the Public Research and Capacity Building Projects of Department of Guangdong Province (2017A010103022), Natural Science Foundation of Guangdong Province (2017A030313079) and Science Foundation funded project of Guangdong Medical University (Z2016001 and M2016023) and Thanks for Prof. S. R. Batten for structure analysis.

References

1 (*a*) M. D. Allendorf, C. A. Bauer, R. K. Bhakta and R. J. T. Houk, *Chem. Soc. Rev.*, 2009, **38**, 1330; (*b*) J. Heine and K. M. Buschbaum, *Chem. Soc. Rev.*, 2013, **42**, 9232; (*c*) X. D. Zhang, Y. F. Gao, H. T. Liu and Z. L. Liu, *CrystEngComm*, 2015, **17**, 6037.

2 (*a*) L. Liu, X. Chen, J. Qiu and C. Hao, *Dalton Trans.*, 2015, **44**, 2897; (*b*) G. A. Eiceman and J. A. Stone, *Anal. Chem.*, 2004, **76**, 390; (*c*) M. E. Germain and M. J. Knapp, *Chem. Soc. Rev.*, 2009, **38**, 2543; (*d*) D. B. Hall, R. E. Holmlin and J. K. Barton, *Nature*, 1996, **382**, 731.

3 (*a*) S. W. Thomas, G. D. Joly and T. M. Swager, *Chem. Rev.*, 2007, **107**, 1339; (*b*) X. Liu, Z. Xiao, J. Xu, W. Xu, P. Sang, L. Zhao, H. Zhu, D. Sun and W. Guo, *J. Mater. Chem. A*, 2016, **4**, 13844; (*c*) J. R. Li, J. Sculley and H. C. Zhou, *Chem. Rev.*, 2012, **112**, 869; (*d*) B. L. Chen, S. Xiang and G. Qian, *Acc. Chem. Res.*, 2010, **43**, 1115.

4 L. E. Kreno, K. Leong, O. K. Farha, M. Allendorf, D. R. P. Van and J. T. Hupp, *Chem. Rev.*, 2012, **112**, 1105.

5 (*a*) L. Di, J. J. Zhang, S. Q. Liu, J. Ni, H. Zhou and Y. J. Sun, *Cryst. Growth Des.*, 2016, **16**, 4539; (*b*) Z. J. Lin, J. Lu, M. Hong and R. Cao, *Chem. Soc. Rev.*, 2014, **43**, 5867; (*c*) N. Stock and S. Biswas, *Chem. Rev.*, 2012, **112**, 933.

6 (*a*) J. Wang, Y. Li, M. Jiang, Y. Liu, L. Zhang and P. Wu, *Chem.–Eur. J.*, 2016, **22**, 13023; (*b*) W. Lu, Z. Wei, Z. Y. Gu, T. F. Liu, J. Park, J. Park, J. Tian, M. Zhang, Q. Zhang, T. Gentle, M. Bosch and H. C. Zhou, *Chem. Soc. Rev.*, 2014, **43**, 5561; (*c*) H. C. Zhou and S. Kitagawa, *Chem. Soc. Rev.*, 2014, **43**, 5415; (*d*) A. J. Lan, K. H. Li, H. H. Wu, D. H. Olson, T. J. Emge, W. Ki, M. C. Hong and J. Li, *Angew. Chem., Int. Ed.*, 2009, **48**, 2334.

7 G. J. Zhao and K. L. Han, *Acc. Chem. Res.*, 2012, **45**, 404.

8 B. L. Chen, S. Ma, F. Zapata, E. B. Lobkovsky and J. Yang, *Inorg. Chem.*, 2006, **45**, 5718.

9 (*a*) B. Gole, A. K. Bar and P. S. Mukherjee, *Chem.–Eur. J.*, 2014, **20**, 2276; (*b*) Z. C. Hu, B. J. Deibert and J. Li, *Chem. Soc. Rev.*, 2014, **43**, 5815.

10 Y. Cui, Y. Yue, G. Qian and B. L. Chen, *Chem. Rev.*, 2012, **112**, 1126.

11 (*a*) E. Haque, J. W. Jun and S. H. Jhung, *J. Hazard. Mater.*, 2011, **185**, 507; (*b*) M. Liang and J. Chen, *Chem. Soc. Rev.*, 2013, **42**, 3453; (*c*) W. Fan, W. Gao, C. Zhang, W. W. Tjiu, J. Pan and T. Liu, *J. Mater. Chem.*, 2012, **22**, 25108.

12 (*a*) Y. Al-Degs, M. A. M. Khraisheh, S. J. Allen and M. N. Ahmad, *Water Res.*, 2000, **34**, 927; (*b*) A. G. Espantaléon, J. A. Nieto, M. Fernández and A. Marsal, *Appl. Clay Sci.*, 2003, **24**, 105; (*c*) C. K. Lee, S. S. Liu, L. C. Juang, C. C. Wang, K. S. Lin and M. D. Lyu, *J. Hazard. Mater.*, 2007, **147**, 997; (*d*) Y. Yu, Y. Y. Zhuang, Y. Li and M. Q. Qiu, *Ind. Eng. Chem. Res.*, 2002, **41**, 1589.

13 T. Gadzikwa, O. K. Farha, C. D. Malliakas, M. G. Kanatzidis, J. T. Hupp and S. T. Nguyen, *J. Am. Chem. Soc.*, 2009, **131**, 13613.

14 (*a*) J. Q. Liu, G. L. Liu, C. Y. Gu, W. C. Liu, J. W. Xu, B. H. Li and W. J. Wang, *J. Mater. Chem. A*, 2016, **4**, 11630; (*b*) J. Q. Liu, J. Wu, F. M. Li, W. C. Liu, B. H. Li, J. Wang, Q. L. Li, R. Yadav and A. Kumar, *RSC Adv.*, 2016, **6**, 31161; (*c*) B. H. Li, J. Wu, J. Q. Liu, C. Y. Gu, J. W. Xu, M. M. Luo, R. Yadav, A. Kumar and S. R. Batten, *ChemPlusChem*, 2016, **81**, 885; (*d*) J. Q. Liu, G. P. Li, W. C. Liu, Q. L. Li, B. H. Li, R. W. Gable, L. Hou and S. R. Batten, *ChemPlusChem*, 2016, **81**, 1299; (*e*) J. Wang, X. R. Wu, J. Q. Liu, B. H. Li, A. Singh, A. Kumar and S. R. Batten, *CrystEngComm*, 2017, **19**, 3519; (*f*) L. Lu, J. Wang, B. Xie, J. Q. Liu, R. Yadav, A. Singh and A. Kumar, *New J. Chem.*, 2017, **41**, 3537.

15 G. M. Sheldrick, *Acta Crystallogr., Sect. A: Found. Adv.*, 2015, **7**, 3.

16 A. L. Spek, *J. Appl. Crystallogr.*, 2003, **36**, 7.

17 (*a*) A. D. Becke, *J. Chem. Phys.*, 1993, **98**, 5648; (*b*) C. T. Lee, W. T. Yang and R. G. Parr, *Phys. Rev. B: Condens. Matter Mater. Phys.*, 1998, **37**, 785; (*c*) M. J. Frisch, G. W. Trucks, H. B. Schlegel, G. E. Scuseria, M. A. Robb, J. R. Cheeseman, J. A. Montgomery, T. Vreven Jr, K. N. Kudin, J. C. Burant, J. M. Millam, S. S. Iyengar, J. Tomasi, V. Barone, B. Mennucci, M. Cossi, G. Scalmani, N. Rega, G. A. Petersson, H. Nakatsuji, M. Hada, M. Ehara, K. Toyota, R. Fukuda, J. Hasegawa, M. Ishida, T. Nakajima, Y. Honda, O. Kitao, H. Nakai, M. Klene, X. Li, J. E. Knox, H. P. Hratchian, J. B. Cross, V. Bakken, C. Adamo, J. Jaramillo, R. Gomperts, R. E. Stratmann, O. Yazyev, A. J. Austin, R. Cammi, C. Pomelli, J. W. Ochterski, P. Y. Ayala, K. Morokuma, G. A. Voth, P. Salvador, J. J. Dannenberg, V. G. Zakrzewski, S. Dapprich,

A. D. Daniels, M. C. Strain, O. Farkas, D. K. Malick, A. D. Rabuck, K. Raghavachari, J. B. Foresman, J. V. Ortiz, Q. Cui, A. G. Baboul, S. Clifford, J. Cioslowski, B. B. Stefanov, G. Liu, A. Liashenko, P. Piskorz, I. Komaromi, R. L. Martin, D. J. Fox, T. Keith, M. A. Al-Laham, C. Y. Peng, A. Nanayakkara, M. Challacombe, P. M. W. Gill, B. Johnson, W. Chen, W. M. Wong, C. Gonzalez and J. A. Pople, Gaussian, Inc., Wallingford CT, 2009.

18 J. K. Schnobrich, O. Lebel, K. A. Cychosz, A. Dailly and A. J. Matzger, *J. Am. Chem. Soc.*, 2010, **132**, 13941.

19 (*a*) S. Yang, X. Lin, A. J. Blake, G. S. Walker, P. Hubberstey, N. R. Champness and M. Schröder, *Nat. Chem.*, 2009, **1**, 487; (*b*) M. Li, D. Li, M. O'Kee and O. M. Yaghi, *Chem. Rev.*, 2014, **114**, 1343; (*c*) X. Lin, I. Telepeni, A. J. Blake, A. Dailly, C. M. Brown, J. M. Simmons, M. Zoppi, G. S. Walker, K. M. Thomas, T. J. Mays, P. Hubberstey, N. R. Champness and M. Schröder, *J. Am. Chem. Soc.*, 2009, **131**, 2159; (*d*) X. Rao, J. Cai, J. Yu, Y. He, C. Wu, W. Zhou, T. Yildirim, B. Chen and G. Qian, *Chem. Commun.*, 2013, **49**, 6719.

20 (*a*) Y. Cui, Y. Yue, G. Qian and B. Chen, *Chem. Rev.*, 2012, **112**, 1126; (*b*) M. D. Allendorf, C. A. Bauer, R. K. Bhakta and R. J. T. Houk, *Chem. Soc. Rev.*, 2009, **38**, 1330; (*c*) K. Jayaramulu, P. Kanoo, S. J. George and T. K. Maji, *Chem. Commun.*, 2010, **46**, 7906; (*d*) R. C. Huxford, J. D. Rocca and W. B. Lin, *Curr. Opin. Chem. Biol.*, 2010, **14**, 262.

21 (*a*) K. Jayaramulu, R. P. Narayanan, S. J. George and T. K. Maji, *Inorg. Chem.*, 2012, **51**, 10089; (*b*) J. K. Ayaramulu, P. Kanoo, S. J. George and T. K. Maji, *Chem. Commun.*, 2010, **46**, 7906.

22 (*a*) X. H. Zhou, L. Li, H. H. Li, A. Li, T. Yang and W. Huang, *Dalton Trans.*, 2013, **42**, 12403; (*b*) Y. Chen, Z. Li, Q. Liu, Y. Shen, X. Wu, D. Xu, X. Ma, L. Wang, Q. H. Chen, Z. Zhang and S. Xiang, *Cryst. Growth Des.*, 2015, **15**, 3847; (*c*) X. D. Zhu, Y. Li, W. X. Zhou, R. M. Liu, Y. J. Ding, J. Lü and D. M. Proserpiocd, *CrystEngComm*, 2016, **18**, 4530.

23 (*a*) S. Sanda, S. Parshamoni, S. Biswas and S. Konar, *Chem. Commun.*, 2015, **51**, 6576; (*b*) L. H. Cao, F. Shi, W. M. Zhang, S. Q. Zang and T. C. W. Mak, *Chem.–Eur. J.*, 2015, **21**, 15705; (*c*) D. K. Singha, S. Bhattachary, P. Majee, S. K. Mondal, M. Kumara and P. Mahata, *J. Mater. Chem. A*, 2014, **2**, 20908; (*d*) Z. Q. Shi, Z. J. Guo and H. G. Zheng, *Chem. Commun.*, 2015, **51**, 8300; (*e*) S. S. Nagarkar, B. Joarder, A. K. Chaudhari, S. Mukherjee and S. K. Ghosh, *Angew. Chem., Int. Ed.*, 2013, **52**, 2881; (*f*) S. S. Nagarkar, A. V. Desai and S. K. Ghosh, *Chem. Commun.*, 2014, **50**, 8915; (*g*) B. Gole, A. K. Bar and P. S. Mukherjee, *Chem.–Eur. J.*, 2014, **20**, 2276; (*h*) S. R. Zhang, D. Y. Du, J. S. Qin, S. J. Bao, S. L. Li, W. W. He, Y. Q. Lan, P. Shen and Z. M. Su, *Chem.–Eur. J.*, 2014, **20**, 3589; (*i*) Y. N. Gong, Y. L. Huang, L. Jiang and T. B. Lu, *Inorg. Chem.*, 2014, **53**, 9457.

24 (*a*) X. Zhou, H. Li, H. Xiao, L. Li, Q. Zhao, T. Yang, J. Zuo and W. Huang, *Dalton Trans.*, 2013, **42**, 5718; (*b*) L. Sun, H. Xing, J. Xu, Z. Liang, J. Yu and R. Xu, *Dalton Trans.*, 2013, **42**, 5508; (*c*) X. Guo, G. Zhu, Q. Fang, M. Xue, G. Tian, J. Sun, X. Li and S. Qiu, *Inorg. Chem.*, 2005, **44**, 3850; (*d*) S. Barman, J. Anand Garg, O. Blacque, K. Venkatesan and H. Berke, *Chem. Commun.*, 2012, **48**, 11127.

25 C. Zhang, L. Sun, Y. Yan, J. Li, X. Song, Y. Liu and Z. Liang, *Dalton Trans.*, 2015, **44**, 230.

26 (*a*) X. Z. Song, S. Y. Song, S. N. Zhao, Z. M. Hao, M. Zhu, X. Meng, L. L. Wu and H. J. Zhang, *Adv. Funct. Mater.*, 2014, **24**, 4034; (*b*) J. D. Xiao, L. G. Qiu, F. Ke, Y. P. Yuan, G. S. Xu, Y. M. Wang and X. Jiang, *J. Mater. Chem. A*, 2013, **1**, 8745.

27 L. V. Meyer, F. Schönfeld and K. Müller-Buschbaum, *Chem. Commun.*, 2014, **50**, 8093.

28 (*a*) Y. Zhou, H. H. Chen and B. Yan, *J. Mater. Chem. A*, 2014, **2**, 13691; (*b*) C. X. Yang, H. B. Ren and X. P. Yan, *Anal. Chem.*, 2013, **85**, 7441; (*c*) S. Pramanik, C. Zheng, X. Zhang, T. J. Emge and J. Li, *J. Am. Chem. Soc.*, 2011, **133**, 4153; (*d*) S. Xiang, W. Zhou, Z. Zhang, M. A. Green, Y. Liu and B. Chen, *Angew. Chem., Int. Ed.*, 2010, **49**, 4615.

29 (*a*) J. Zhang, B. Zheng, T. T. Zhao, G. H. Li, Q. S. Huo and Y. L. Liu, *Cryst. Growth Des.*, 2014, **14**, 2394; (*b*) J. Wang, Y. Li, M. Jiang, Y. H. Liu, L. W. Zhang and P. Y. Wu, *Chem.–Eur. J.*, 2016, **22**, 13023.

30 J. S. Qin, S. R. Zhang, D. Y. Du, P. Shen, S. J. Bao, Y. Q. Lan and Z. M. Su, *Chem.–Eur. J.*, 2014, **20**, 5625.

31 X. Zhang, Y. Gao, H. Liu and Z. Liu, *CrystEngComm*, 2015, **17**, 6037.

32 S. Legergren, About the Theory of so-Called Adsorption of Soluble Substances, *K. Sven. Vetenskapsakad. Handl.*, 1898, **24**, 1.

33 Y. S. Ho and G. McKay, *Process Biochem.*, 1999, **34**, 451.

34 Y. S. Ho, *Water Res.*, 2006, **40**, 119.

35 W. J. Weber and J. C. Morris, *J. Sanit. Eng. Div., Am. Soc. Civ. Eng.*, 1963, **89**, 31.

36 L. Liu, Z. Y. Gao, X. P. Su, X. Chen, L. Jiang and J. M. Yao, *ACS Sustainable Chem. Eng.*, 2015, **3**, 432.